Journal of Materials Chemistry C

ROYAL SOCIETY OF CHEMISTRY

PAPER

View Article Online
View Journal | View Issue

Cite this: J. Mater. Chem. C, 2025, 13, 14465

Luminescent solar concentrators based on environmentally friendly tripodal D–(pi–A)$_3$ triarylamine luminophores†

Elisavet Tatsi,‡[a] Venanzio Raglione,‡[b] Gaia Roberta Ragno,[a] Stefano Turri,[a] Giuseppe Mattioli,[c] Francesco Porcelli,[c] Daniela Caschera,[d] Chiara Botta,[e] Gloria Zanotti *[c] and Gianmarco Griffini *[a]

Luminescent solar concentrators (LSCs) offer a promising approach for efficient solar light harvesting and energy conversion, while possessing favorable aesthetic characteristics that make them particularly interesting for integration in the built environment. Although this technology has witnessed enormous progress in the past decade, different open challenges still interfere with the large-scale use of LSCs, including the limited spectral absorption of luminophores, the presence of non-negligible photon reabsorption losses, and the limited photostability of materials and devices. Star-shaped triphenylamine derivatives emerge as promising luminophore candidates due to their tunable optical properties and synthetic versatility. This study introduces a series of tris-(4-phenylethynyl-phenyl)-amine-based molecules with varied peripheral groups, obtained at room temperature through a sustainable multistep synthetic method characterized by an E-factor <190. The symmetrical D–(π–A)$_3$ structure of these molecules is designed to enhance their optical response in view of their application as luminescent species in LSCs, as also corroborated by density functional theory calculations. Their incorporation in poly(methyl methacrylate) matrices at increasing concentration enables the systematic investigation of their optical characteristics and their photonic and photovoltaic response in LSC devices under simulated sunlight, demonstrating high average visible transmittance (~90%) and maximum internal and external photonic efficiencies as high as ~50% and ~5%, respectively. The particularly straightforward and affordable synthetic pathway developed to achieve these luminophores, together with the excellent performance of the corresponding LSC devices and their favorable aesthetic characteristics, make these systems promising candidates for future building-integrated LSC applications. In particular, their narrow absorption bands and high photoluminescence efficiencies make them especially promising for applications in transparent LSCs, where high visible light transmittance is prioritized over broad absorption, alongside energy harvesting.

Received 16th April 2025,
Accepted 31st May 2025

DOI: 10.1039/d5tc01559f

rsc.li/materials-c

1. Introduction

Luminescent solar concentrators (LSCs) represent a promising technology for efficient solar light harvesting and photon energy conversion. By leveraging luminescent materials embedded in a transparent matrix, LSCs offer a cost-effective means of capturing and concentrating incident light, which can then be converted into electricity when photovoltaic (PV) cells are connected to the device. However, the LSC technology still faces several significant challenges that limit its widespread adoption in real-life scenarios. Among these, reabsorption losses occur when the light emitted from a luminescent center is reabsorbed by the same or by a nearby luminophore molecule within the system, thus reducing the amount of light successfully waveguided to the edge-coupled solar cells and leading to a drop in the

[a] Department of Chemistry, Materials and Chemical Engineering "Giulio Natta", Politecnico di Milano, Piazza Leonardo da Vinci 32, 20133 Milano, Italy. E-mail: gianmarco.griffini@polimi.it
[b] Istituto di Struttura della Materia (ISM), Consiglio Nazionale delle Ricerche (CNR), via Fosso del Cavaliere 100, 00133 Roma, Italy
[c] Istituto di Struttura della Materia (ISM), Consiglio Nazionale delle Ricerche (CNR), Strada provinciale 35d/9, 00010 Montelibretti, Rm, Italy. E-mail: gloria.zanotti@mlib.ism.cnr.it
[d] Istituto per lo Studio dei Materiali Nanostrutturati (ISMN), Consiglio Nazionale delle Ricerche (CNR), Strada provinciale 35d/9, 00010 Montelibretti, Rm, Italy
[e] Institute of Sciences and Chemical Technologies "Giulio Natta" (SCITEC) of CNR, via A. Corti 12, 20133 Milano, Italy

† Electronic supplementary information (ESI) available. See DOI: https://doi.org/10.1039/d5tc01559f

‡ Equal contribution.

maximum photon emission efficiency.[1–4] In addition to the optical losses due to photon reabsorption, prolonged light exposure can also significantly affect the performance of LSC devices during operation. Indeed, continuous solar illumination may lead to degradation of the luminescent species and of the host matrix material through radical pathways activated by the action of harmful UV photons, ultimately yielding reduced photoluminescence response.[5] As a result, the design and development of optically performing and robust materials for LSCs represents a key milestone for the advancement of this technology.

To meet these pressing challenges, recent research in the field has developed various strategies addressing both the luminophore and the host matrix systems, including the synthesis of quantum dots (QDs)[6–8] with large Stokes shifts to minimize reabsorption, the development of robust self-healing polymeric matrices[9,10] for enhanced durability, the design of organic fluorophores[11–13] and donor–acceptor (D–A)[2,14–16] systems exploiting the Förster resonance energy transfer (FRET) process to widen the absorption spectrum while minimizing reabsorption losses, and the incorporation of aggregation-induced emitters luminogens (AIE*gens*).[17–19]

A particularly interesting class of luminophore not extensively utilized in LSCs[20–22] is that of star-shaped derivatives of triphenylamine (TPA), which have shown great promise due to their synthetic versatility and favorable optical characteristics.[23–25] Indeed, they allow for extreme fine-tuning of their chemical and optoelectronic properties as the parent TPA core can be tailored through either symmetrical or unsymmetrical substitutions.[26–28] Additionally, TPA derivatives benefit from accessible and adaptable chemistry, with functionalization strategies that leverage the rich chemistry of aromatic compounds and facilitate the formation of multi-branched donor–bridge–acceptor ($D(-\pi-A)_3$) systems.[29] Moreover, the non-planarity of the TPA core enhances the solubility of its derivatives, contributing to generally good processability.[30] Lastly, the starting materials are available at reasonable prices from commercial suppliers, making it a cost-effective option. Given the outstanding tunability of their properties, triarylamines are widely studied in cutting-edge technologies such as organic and perovskite-based PVs[31,32] as well as in biological applications like cell imaging.[33] Recent research has capitalized on these properties, leading to the development of preliminary examples of TPA-based LSCs incorporating D–A pairs for FRET,[22,34,35] TPA-derivatives with high photoluminescence quantum yields (PLQY),[36,37] and TPA-based AIE systems.[36,38,39]

Following this groundwork, this study explores a series of functionalized tris-(4-phenylethynyl-phenyl)-amine-based luminescent molecules, featuring a symmetrical $D-(\pi-A)_3$ donor–acceptor structure.[40] This design enhances their photoluminescence properties while keeping synthetic complexity low, making them well-suitable for implementation in LSC devices. With the aim to identify increasingly effective and less impactful synthetic conditions, three different TPA-derivatives (TP-6CF3, TP-3COOHex, and TP-6CN, bearing 3,5-bis(trifluoromethyl)phenyl, hexyl-4-benzoate, and 3,4 dicyanophenyl moieties, respectively) were synthesized in the presence of propane-1,2-diol – a non-toxic, non-volatile and biodegradable substance with minimum environmental impact, produced through the modification of glycerol[41,42] or by microbial synthesis processes[43] – as the primary reaction medium. This approach, coupled with ambient-temperature conditions throughout the entire three-step synthetic pathway, represents a significant progress in the direction of more sustainable synthetic protocols for the development of optically-active functional molecules. The photophysical properties of the three target derivatives in solution were investigated experimentally across several solvents and correlated to the different functionalization patterns of the TPA core. In addition, density functional theory (DFT) calculations were carried out to establish clear relationships between molecular arrangement and optical properties. Finally, the incorporation of such TPA-based derivatives in poly(methyl methacrylate) – PMMA matrices at increasing concentration enabled the systematic investigation of their photonic and PV response, shedding light on their potential as alternative luminophores for efficient LSC systems.

2. Experimental

2.1 Materials

PMMA (ALTUGLAS BS 550) was purchased from Arkema. Monocrystalline high efficiency silicon solar cells (mc-Si PV cells) were provided by IXYS (IXOLAR SolarBIT KXOB22-12 × 1F, active area 2.2 × 0.6 cm^2, V_{OC} = 0.64 ± 0.01 V, J_{SC} = 42.60 ± 0.42 mA cm^{-2}, FF = 69.4 ± 0.3%, power conversion efficiency = 18.69 ± 0.23%).

All the reagents were used as received from commercial suppliers. Reactions were purged and refilled three times, performed under argon and monitored by thin-layer chromatography (TLC) employing a polyester layer coated with 250 mm F254 silica gel.

2.2 Synthesis of triarylamine-based derivatives

2.2.1 Tris(4-((trimethylsilyl)ethynyl)phenyl)amine (TP-3TMSA). A solution of tris(4-iodophenyl)amine (1 g, 1.6 mmol, 1.0 eq.), $Pd(PPh_3)_4$ (0.092 g, 0.08 mmol, 0.05 eq.), CuI (0.001 g, 0.005 mmol, 0.003 eq.), triethylamine (3 mL) was placed in propane-1,2-diol (2 mL) at 0 °C and under inert atmosphere (argon) and allowed to stir for 10 minutes. Then, ethynyltrimethylsilane (0.73 mL, 5.12 mmol, 3.2 eq.) was added over 30 minutes. The reaction was stirred for 1d, then treated with 5 mL of HCl 1 M, diluted with 45 mL of water to precipitate the crude and filtered on Büchner. Purification by washing with cold ethyl acetate afforded the product as a white/pale yellow solid with a yield of 96%. m.p. 170–171 °C. ^{1}H NMR (600 MHz, $CDCl_3$) δ 7.34 (d, J = 8.7 Hz, 6H), 6.96 (d, J = 8.7 Hz, 6H), 0.24 (s, 27H). ^{13}C NMR (151 MHz, $CDCl_3$) δ 146.80, 133.17, 123.82, 117.84, 104.87, 93.97, 0.01.

2.2.2 Tris(4-ethynylphenyl)amine (TETPA). To a solution of 0.2 g of tris(4-((trimethylsilyl)ethynyl)phenyl)amine (0.37 mmol, 1 eq.) in MeOH/DCM = 1 : 1 (10 mL) 0.24 g of K_2CO_3 (1.74 mmol, 4.6 eq.) was added and the resulting mixture was stirred for 4 hours at room temperature under argon atmosphere. The solution was then diluted with 5 mL of water and filtered on

Büchner. After washing with a further 15 mL of water the crude product was pure and it has been used without any further purifications. White/yellowish solid. 0.115 g, Yield 98%. m.p. 109–110 °C. ^{1}H NMR (600 MHz, $CDCl_3$) δ 7.38 (d, J = 8.7 Hz, 6H), 7.01 (d, J = 8.7 Hz, 6H), 3.06 (s, 3H). ^{13}C NMR (151 MHz, CDCl3) δ 147.05, 133.38, 123.95, 116.90, 83.41.

2.2.3 Tris(4-((4-(trifluoromethyl)phenyl)ethynyl)phenyl)amine (TP-6CF3). 1-Iodo-3,5-bis(trifluoromethyl)benzene (0.084 mL, 0.47 mmol, 3.2 eq.) was dispersed in glycerol (or propane-1,2-diol) (2 mL) at room temperature and under an inert atmosphere (argon). Then $Pd(PPh_3)_4$ (0.009 g, 0.008 mmol, 0.05 eq.), triethylamine (3 mL), tris(4-ethynylphenyl)amine (0.050 g, 0.16 mmol, 1 eq.), and CuI (0.002 g, 0.008 mmol, 0.05 eq.) were added sequentially. The reaction appeared to be over in 30 min; however, it was stirred vigorously (1000 rpm) for 4 hours. Then the reaction mixture was washed with H_2O/HCl 1 M solution (15 + 5) mL and filtered on Büchner. Recrystallization of the filtrate in DCM afforded 111 mg (131 mg in propane-1,2-diol) of the product as a yellow solid with a yield of 73% (87% in propane-1,2-diol). When propane-1,2-diol was used as the solvent, the purification was performed by column chromatography using 4 g of silica gel as the stationary phase and 50 mL of hexane as the eluent. m.p. 283 °C (dec.). ^{1}H NMR (600 MHz, CD_2Cl_2) δ 8.00 (s, 6H), 7.86 (s, 3H), 7.53 (d, J = 8.8 Hz, 6H), 7.16 (d, J = 8.8 Hz, 6H). ^{13}C NMR (151 MHz, CD_2Cl_2) δ 147.31, 133.15, 131.86, 131.64, 131.36, 130.28, 128.02, 125.76, 124.24, 121.41, 116.79, 92.54, 86.27. MALDI-TOF m/z calcd: 953.1387 found: 953.094.

2.2.4 Tris(4-((4-(trifluoromethyl)phenyl)ethynyl)phenyl)amine (TP-6CF3). 1-Iodo-3,5-bis(trifluoromethyl)benzene (0.084 mL, 0.47 mmol, 3.2 eq.) was dispersed in glycerol (or propane-1,2-diol) (2 mL) at room temperature and under an inert atmosphere (argon). Then $Pd(PPh_3)_4$ (0.009 g, 0.008 mmol, 0.05 eq.), triethylamine (3 mL), tris(4-ethynylphenyl)amine (0.050 g, 0.16 mmol, 1 eq.), and CuI (0.002 g, 0.008 mmol, 0.05 eq.) were added sequentially. The reaction appeared to be over in 30 min; however, it was stirred vigorously (1000 rpm) for 4 hours. Then the reaction mixture was washed with H_2O/HCl 1 M solution (15 + 5) mL and filtered on Büchner. Recrystallization of the filtrate in DCM afforded 111 mg (131 mg in propane-1,2-diol) of the product as a yellow solid with a yield of 73% (87% in propane-1,2-diol). When propane-1,2-diol was used as the solvent, the purification was performed by column chromatography using 4 g of silica gel as the stationary phase and 50 mL of hexane as the eluent. m.p. 283 °C (dec.). ^{1}H NMR (600 MHz, CD_2Cl_2) δ 8.00 (s, 6H), 7.86 (s, 3H), 7.53 (d, J = 8.8 Hz, 6H), 7.16 (d, J = 8.8 Hz, 6H). ^{13}C NMR (151 MHz, CD_2Cl_2) δ 147.31, 133.15, 131.86, 131.64, 131.36, 130.28, 128.02, 125.76, 124.24, 121.41, 116.79, 92.54, 86.27. MALDI-TOF m/z calcd: 953.1387 found: 953.094.

2.2.5 Trihexyl 4,4′,4″-((nitrilotris(benzene-4,1-diyl))tris(ethyne-2,1-diyl))tribenzoate (TP-3COOHex). To a solution of hexyl 4-iodobenzoate (0.168 g, 0.51 mmol, 3.2 eq.) in glycerol (or propane-1,2-diol) (2 mL) at room temperature and under inert atmosphere (argon) was added sequentially $Pd(PPh_3)_4$ (0.009 g, 0.008 mmol, 0.05 eq), triethylamine (3 mL), tris(4-ethynylphenyl)amine (0.05 g, 0.16 mmol, 1 eq.), and CuI (0.002 g, 0.008 mmol, 0,05 eq.). The reaction appeared to be over in 30 min; however, it was stirred vigorously (1000 rpm) for 4 hours. Then the reaction mixture was washed with H_2O/HCl 1 M solution (15 + 5) mL and filtered on Büchner. Recrystallization of the filtrate in hexane/DCM afforded 61 mg (106 mg in propane-1,2-diol) of the product as a brilliant green/yellow solid with a yield of 41% (72% in propane-1,2-diol). When propane-1,2-diol was used as the solvent, the purification was performed by column chromatography using 4 g of silica gel as the stationary phase and 50 mL of petroleum ether/tetrahydrofuran = 9 : 1 as the eluent. mp 162–164 °C. ^{1}H NMR (600 MHz, CD_2Cl_2) δ 8.03 (d, J = 8.4 Hz, 6H), 7.60 (d, J = 8.4 Hz, 6H), 7.50 (d, J = 8.6 Hz, 6H), 7.13 (d, J = 8.6 Hz, 6H), 4.32 (t, J = 6.7 Hz, 6H), 1.84–1.72 (m, 6H), 1.51–1.42 (m, 6H), 1.40–1.33 (m, 14H), 0.93 (t, J = 7.0 Hz, 7H). ^{13}C NMR (151 MHz, CD_2Cl_2) δ 165.87, 147.02, 132.96, 131.29, 129.95, 129.39, 127.84, 124.16, 117.49, 92.04, 88.54, 65.27, 31.47, 28.65, 25.70, 22.55, 13.76. MALDI-TOF m/z calcd: 929.4655 found: 929.451.

2.2.6 4,4′,4″-((Nitrilotris(benzene-4,1-diyl))tris(ethyne-2,1-diyl))triphthalonitrile (TP-6CN). 4-Iodophthalonitrile (0.129 g, 0.51 mmol, 3.2 eq.) was dissolved in glycerol (or propane-1,2-diol) (2 mL) at room temperature under an inert atmosphere (argon). Then $Pd(PPh_3)_4$ (0.009 g, 0.008 mmol, 0.05 eq.), triethylamine (3 mL), tris(4-ethynylphenyl)amine (0.050 g, 0.16 mmol, 1 eq.), and CuI (0.002 g, 0.008 mmol, 0.05 eq.) were added. The reaction appeared to be over in 15 min; however, it was stirred vigorously (1000 rpm) for 4 hours. Then the reaction mixture was washed with H_2O/HCl 1 M solution (15 + 5) mL and filtered on Büchner. Recrystallization of the filtrate in hexane/DCM afforded 78 mg (100 mg in propane-1,2-diol) of the product as an orange solid with a yield of 70% (91% in propane-1,2-diol). When propane-1,2-diol was used as the solvent, the purification was performed by column chromatography using 4 g of silica gel as the stationary phase and 25 ml of toluene, then 25 mL of ethyl acetate as the eluent. mp 177–180 °C. ^{1}H NMR (600 MHz, CD_2Cl_2) δ 7.93 (d, J = 1.4 Hz, 3H), 7.84 (dd, J = 8.2, 1.5 Hz, 3H), 7.82 (d, J = 8.2 Hz, 3H), 7.53 (d, J = 8.6 Hz, 6H), 7.16 (d, J = 8.7 Hz, 6H). ^{13}C NMR (151 MHz, CD_2Cl_2) δ 147.54, 135.82, 135.45, 133.56, 129.26, 128.95, 128.14, 124.29, 116.47, 116.24, 115.40, 115.00, 114.03, 96.20, 86.14. MALDI-TOF m/z calcd: 695.1858 found: 695.075.

2.3 Measurements

^{1}H and ^{13}C NMR spectra were recorded on a Bruker AVANCE 600 NMR spectrometer (Rheinstetten, Germany) operating at a proton frequency of 600.13 MHz in $CDCl_3$ or CD_2Cl_2. Chemical shifts (δ) are given in ppm relative to the residual solvent peaks of the deuterated solvents. UV-vis spectra in solution were recorded on a PerkinElmer Lambda 950 UV-vis/NIR spectrophotometer (PerkinElmer Italia, Milano, Italy) using dichloromethane as solvent. MALDI-TOF spectra were recorded at a Toscana Life Science facility in a MALDI-TOF/TOF Ultraflex III (Bruker). Steady-state fluorescence spectra were recorded with a JobinYvon Fluorolog3 spectrofluorometer – no filters were used. All experiments were performed at room temperature using quartz cuvettes with an optical path length of 10 mm. PLQY measurements were conducted using excitation wavelengths of 380 and 400 nm for

TP-6CF3 and TP-3COOHex in all solvents, and for TP-6CN in dichloromethane and tetrahydrofuran, with perylene as the standard. For TP-6CN in acetone, the quantum yield was measured at an excitation wavelength of 440 nm, using rhodamine 6G as the standard. Time-resolved fluorescence measurements were carried out by a time-correlated single-photon-counting (TCSPC) system (Horiba-Jobin-Yvon), using a 405 nm pulsed laser diode and collecting the emission decay at the corresponding maximum emission wavelengths. The fluorescence decay profile was analyzed through decay analysis software (DAS6a HORIBA Scientific). Micrographs of TP-6CF3 were captured through a Leica DMI3000B fluorescence microscope equipped with a digital camera, by using specific filters based on the excitation and emission wavelengths of the investigated sample. UV-vis absorption spectra of TPA/PMMA-based systems were recorded on a Thermo Scientific Evolution 600 UV–vis spectrophotometer using wavelength scan with a resolution of 1 nm at a scan speed of 120 nm min^{-1} and a slit width of 2 nm. Steady-state fluorescence spectroscopy analyses of TPA/PMMA-based systems were performed on a Jasco FP-6600 spectrofluorometer. Internal and external photon efficiency (η_{int} and η_{ext}, respectively) measurements were performed by illuminating the top face of the LSC using an Abet Technologies Sun 2000 solar simulator with AM1.5G filter (irradiance of 1000 W m^{-1}) and by collecting the edge emission of the LSC devices with a spectroradiometer (International Light Technologies ILT950) equipped with a cosine corrector. The emission spectra of the LSCs were recorded using SpectrILight software. For the evaluation of the power conversion efficiency of the LSC-PV assembly, a digital multimeter (KEITHLEY 2612B) was used to perform the voltage scans and measure the current output of the LSC-PV device subjected to 1 Sun AM1.5G top illumination by the same solar simulator used for the photonic characterization. All measurements (both photonic and PV) were conducted against a black background to avoid double-pass of transmitted photons with subsequent performance overestimation. All the above-cited tests were repeated on at least three devices, and the average values (±standard deviation) were reported.

2.4 Preparation of TPA-based/PMMA-LSC in thin-film configuration and LSC-PV assembly

LSCs were fabricated in thin-film configuration starting from $CHCl_3$ solutions of PMMA (10 wt%) with various concentrations of TP-based fluorophores (1–7 wt% with respect to dry polymer). Thin films were obtained by spin coating (900 rpm for 60 s) onto 4.4 × 4.4 × 0.6 cm^3 soda lime glass slabs using a Laurell WS-400BZ-6NPP/LITE instrument. The average coatings thickness was measured by a KLA Tencor P-17 profilometer to be ~4 μm. Also, rectangular-shaped LSCs with dimensions 20.0 × 5.0 × 0.6 cm^3 were fabricated using doctor-blade technique on high-optical-quality N-BK7 glass slabs. The films were fabricated by setting a sliding velocity equal to 2 m min^{-1} and using a bar with a diameter that enables the fabrication of films with a thickness of ~4–6 μm.

The LSC-PV assembly was fabricated by integration of the LSC device with four mc-Si PV cells in a series configuration. Specifically, two opposite edges of the glass substrate were connected to the photoactive regions of two PV cells each. The integration was achieved using a hot-melt thermoplastic polyurethane (TPU) film with a refractive index of ~1.49 (close to the one of the optical glass used). The TPU film was heated until softening, facilitating the optical coupling between the LSC glass substrate and the PV cells. Subsequently, the system was allowed to cool down to room temperature, ensuring a robust mechanical bond between the components. The other two LSC edges were covered with black tape, while no additional mirrors or reflectors were utilized.

2.5 Atomistic simulations

Atomistic simulations of TP-6CF3, TP-3COOHex and TP-6CN were performed using a multi-level protocol. The most stable conformers of the molecules and of their dimers were identified by a conformer-rotamer ensemble sampling tool (CREST) algorithm, which uses the tight-binding GFN2-xTB Hamiltonian as an "engine" for the search of minimum energy configurations. Electronic and optical properties of the most stable conformers were then investigated using (time-dependent) density functional theory simulations, carried out in a GTO framework using the ORCA suite of programs. A detailed description of theoretical methods is provided in the ESI.†

3. Results and discussion

3.1 Synthesis and molecular properties of TPA-based molecules

The synthesis of the target molecules involves three steps: an initial Sonogashira coupling to introduce triple bonds onto the triarylamine core, followed by deprotection to obtain the key intermediate tris(4-ethynylphenyl)amine (TETPA), and finally, functionalization through a second Sonogashira coupling with three aryl iodides (1-iodo-3,5-bis(trifluoromethyl)benzene, hexyl-4-iodobenzoate, and 4-iodophthalonitrile), as sketched in Scheme 1. The TETPA intermediate was obtained in two steps, following the procedure derived from the optimization of the best experimental conditions outlined in the ESI† (Table S1) and illustrated in Scheme 1. Both tris(4-iodophenyl)amine and tris(4-bromophenyl)amine were tested as starting precursors. During this process, an extensive investigation of experimental parameters such as the order of reagents addition, temperature, and solvents was systematically performed. Interestingly, the Sonogashira coupling of 4-iodotriphenylamine and trimethylsilylacetylene in propane-1,2-diol resulted in the formation of the intermediate TP-3TMSA with an exceptionally high yield of 96% on a 1-gram scale even at room temperature, surpassing those obtained using standard solvents at higher reaction temperatures. The subsequent cleavage of the trimethylsilyl groups afforded TETPA with an almost quantitative yield.[44]

With the aim to further increase yield while boosting eco-friendliness with respect to recent literature findings,[40] we focused on improving the second Sonogashira coupling step. To enhance compliance with the main green chemistry

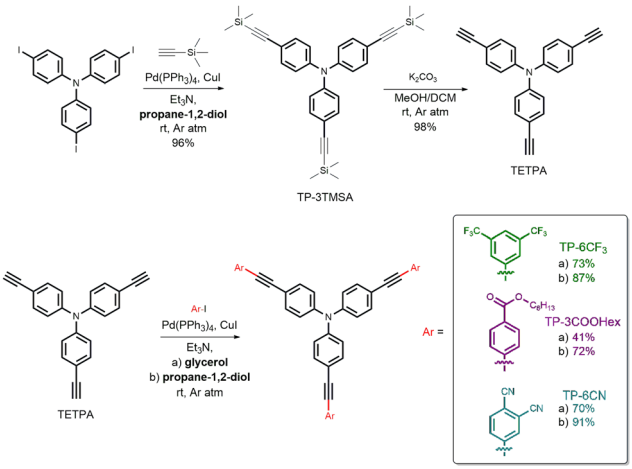

Scheme 1 Synthetic routes for the synthesis of TPA-based molecules.

principles, such as avoiding heat-intensive experimental conditions throughout the entire synthesis, we evaluated both glycerol and propane-1,2-diol as low-temperature reaction media, relying on the generally good reactivity of aryl iodides at room temperature. Tetrakis(triphenylphosphine)palladium ($Pd(PPh_3)_4$) acted as the catalyst in all reactions, aided by CuI as the cocatalyst and triethylamine as the base. Remarkably, propane-1,2-diol gave the best results for all the derivatives, as reported in Scheme 1, allowing to achieve impressive total yields of 82%, 68%, and 86% for TP-6CF3, TP-3COOHex, and TP-6CN, respectively. To estimate the environmental sustainability of our synthetic protocol, we calculated its environmental factor (E-factor), a green chemistry metric defined as the ratio between the mass of waste produced and the product obtained.[45,46] Notably, we achieved overall E-factors of 151.3, 179.8, and 187.3 for the three compounds (detailed calculations are reported in the ESI,† Section S3), which are especially promising given the multistep nature of our protocol and are consistent with reported metrics for sustainably synthesized Sonogashira-derived architectures (E-factor = 24.9–312.0).[47] The use of propane-1,2-diol as a green solvent and ambient-temperature conditions further underscores the sustainability of this approach compared to traditional routes employing toxic solvents or energy-intensive purifications. The chemical structure of the three molecules was confirmed with ^1H and ^{13}C NMR (Section S2 in the ESI†). Regarding the processability of the compounds in organic media, TP-3COOHex was found to exhibit excellent solubility, being compatible with a wide range of organic solvents. TP-6CF3 could be dissolved only in solvents with moderate or no polarity, such as hexane, and polar solvents like ethyl acetate best dissolve TP-6CN.

3.2 Photophysical characterization

3.2.1 Spectroscopic characterization in solution. The photophysical properties of the TPA-based molecules were studied by UV-vis and fluorescence spectroscopy in different solvents. The results showed that the position of the absorption and emission bands was greatly influenced by the nature of the substituents on the molecules. In particular, the main absorption peak for TP-6CN was red-shifted above 400 nm compared to those of the other two molecules, instead lying at around 375 nm. This shift may be due to the bathochromic effect induced by the cyano groups, which extend the conjugation system of the structure. The photophysical data for all systems are included in Table 1 (corresponding absorption and emission spectra are reported in Section S4 in the ESI†).

Table 1 Photophysical characteristics of TPA-based molecules in different solvents: absorption and fluorescence maxima (λ_{max}); Stokes shift; average lifetime (τ); PLQY

	Solvent	λ_{abs,S_0-S_1} (nm)	λ_{em} (nm)	Stokes shift (eV) [cm^{-1}]	τ (ns)	PLQY
TP-6CF3	THF	376	449	0.53 [4324.03]	1.74	0.67
	DCM	376	445	0.51 [4123.83]	1.77	0.72
	Acetone	376	475	0.69 [5543.11]	2.27	0.54
TP-3COOHex	THF	375	454	0.57 [4640.23]	1.66	0.74
	DCM	375	472	0.68 [5480.23]	2.04	0.77
	Acetone	375	488	0.77 [6174.86]	2.35	0.54
TP-6CN	THF	410	528	0.68 [5450.85]	3.35	0.54
	DCM	418	531	0.63 [5091.05]	3.70	0.53
	Acetone	408	594	0.95 [7674.79]	0.99	0.34

Regarding steady-state photoluminescence, all three molecules exhibited positive solvatochromism with increasing solvent polarity, which may be attributed to an enhanced dipole moment of the excited state interacting with the solvent reaction field. The obtained compounds showed moderate to very high Stokes shifts, with TP-6CN demonstrating a remarkable 0.95 eV value in acetone. The PLQY was measured at excitation wavelengths of 380 nm, 400 nm or 440 nm depending on the emission characteristics of the molecule in the target solvent, using perylene (PLQY = 0.92 in ethanol) or Rhodamine 6G (PLQY = 0.95 in ethanol) as references. In solvents with similar polarity, such as tetrahydrofuran (THF) and dichloromethane (DCM), the three compounds exhibited almost consistent behavior in both PLQY and lifetime decay (τ). However, as solvent polarity increased, a decrease in PLQY was observed, with acetone displaying significantly lower values compared to THF and DCM. Additionally, the τ values showed varying trends. Specifically, TP-3COOHex and TP-6CF3 exhibited longer decay times in acetone, potentially leading to non-radiative decay processes that may account for the observed decrease in PLQY. In contrast, TP-6CN demonstrated a very short decay time in acetone (1 ns), along with the lowest PLQY (0.34). This outcome may be due to the formation of aggregates that quench fluorescence, thereby also reducing the corresponding PLQY.

Simulations rooted on (time dependent) DFT facilitated the understanding and the prediction of the electronic properties at molecular level, focusing in particular on the evaluation of the influence of –CF3, –COOR and –CN groups on the electronic properties of the TPA-based compounds in solution and in the solid state. Oxidation and reduction potentials reported in Fig. 1(A) indicate that the six –CN groups attached to TP-6CN were particularly effective in the stabilization of an excess negative charge, as suggested by the lowest reduction potential, while also participating in the extended conjugation of the

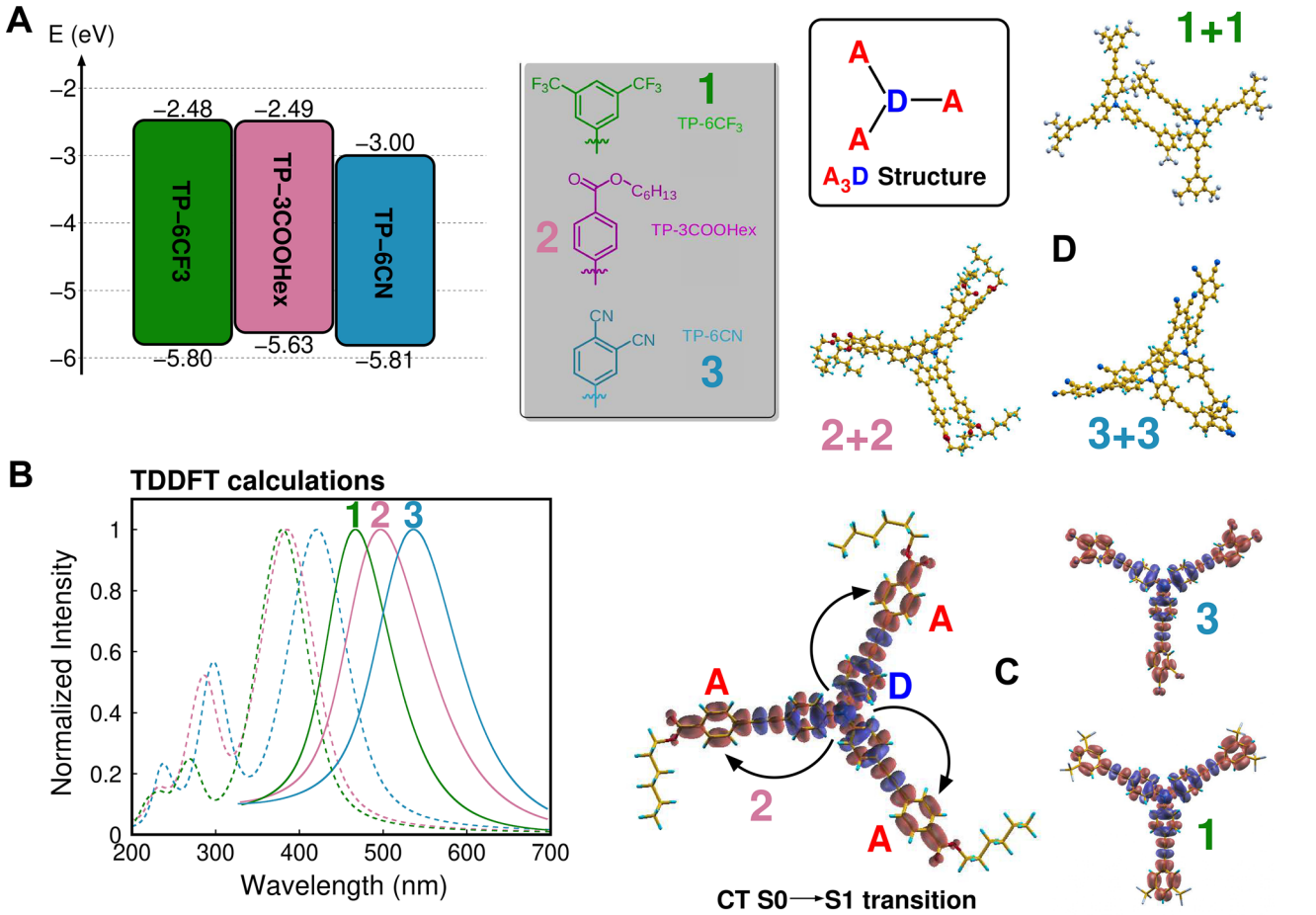

Fig. 1 (TD)DFT results of TP-6CF3 (1), TP-3COOHex (2) and TP-6CN (3). (A) Energy alignment of reduction and oxidation potentials in DCM (0 = vacuum level) of molecules 1–3. (B) TDDFT vibronic absorption (dashed lines) and emission (solid lines) spectra of molecules 1–3. (C) Maps of electronic density difference between the molecular ground state S0 and the first excited singlet state S1 of molecules 1–3; electronic charge is displaced from blue donor regions to red acceptor regions upon excitation of the molecules, as indicated by black arrows in the case of molecule 2, yielding charge-transfer excited states. (D) Optimized DFT structures of the most stable dimers of molecules 1–3.

molecule to yield the lowest optical band gap of 2.95 eV (all calculated data for the three molecules are reported in Table S11 in the ESI†). The calculated absorption spectra reported in Fig. 1(B) were found to be in close agreement with measurements (Fig. 2 and Table 1) and were shown to be dominated by a strong charge-transfer excitation, corresponding almost entirely to an electronic transition between the HOMO (A symmetry) and the degenerate LUMO (E symmetry), as depicted in Fig. S23 in the ESI†). The absorption spectrum peaked in the uppermost section of the visible region in the case of TP-6CN (2.95 eV) and slightly above in the cases of TP-3COOHex and TP-6CF3 (3.22 eV and 3.27 eV, respectively). We compare density difference maps between the S0 and S1 states of TP-6CF3 and TP-3COOHex shown in Fig. 1(C), with that reported for TP-6CN.[40]

All the maps clearly indicate a charge depletion from the amino group at the center of the molecule and a similar corresponding displacement toward the farthest part of the three electron-acceptor branches upon excitation. Such opto-electronic properties of the three molecules induce, in turn, a significant difference between absorption and emission. Theoretical calculations yielded Stokes shifts of 0.64 eV, 0.75 eV and 0.65 eV for TP-6CF3, TP-3COOHex and TP-6CN in DCM solution, slightly overestimated with respect to measurements (see Table 1) but following the same trend, with TP-3COOHex representing the most promising molecule for minimizing reabsorption losses in LSC applications.

As in LSC devices luminophores are typically embedded in a polymeric host matrix by solvent-assisted dissolution/dispersion, our study was extended to the investigation of molecular dimers, to provide information on early stages of molecular aggregation. Such results are, in turn, useful as they can help explaining the behavior of the molecules in solid-state devices. Fig. 1(D) shows the most stable structures of TP-6CF3, TP-3COOHex and TP-6CN dimers, sorted using a Conformers-Rotamers Ensemble Search Tool (CREST) rooted on tight-binding simulations (see ESI† for a detailed description of the computational protocol). Two different interaction patterns were found: in the case of TP-3COOHex and TP-6CN, the interaction was found to be driven by dispersion forces between

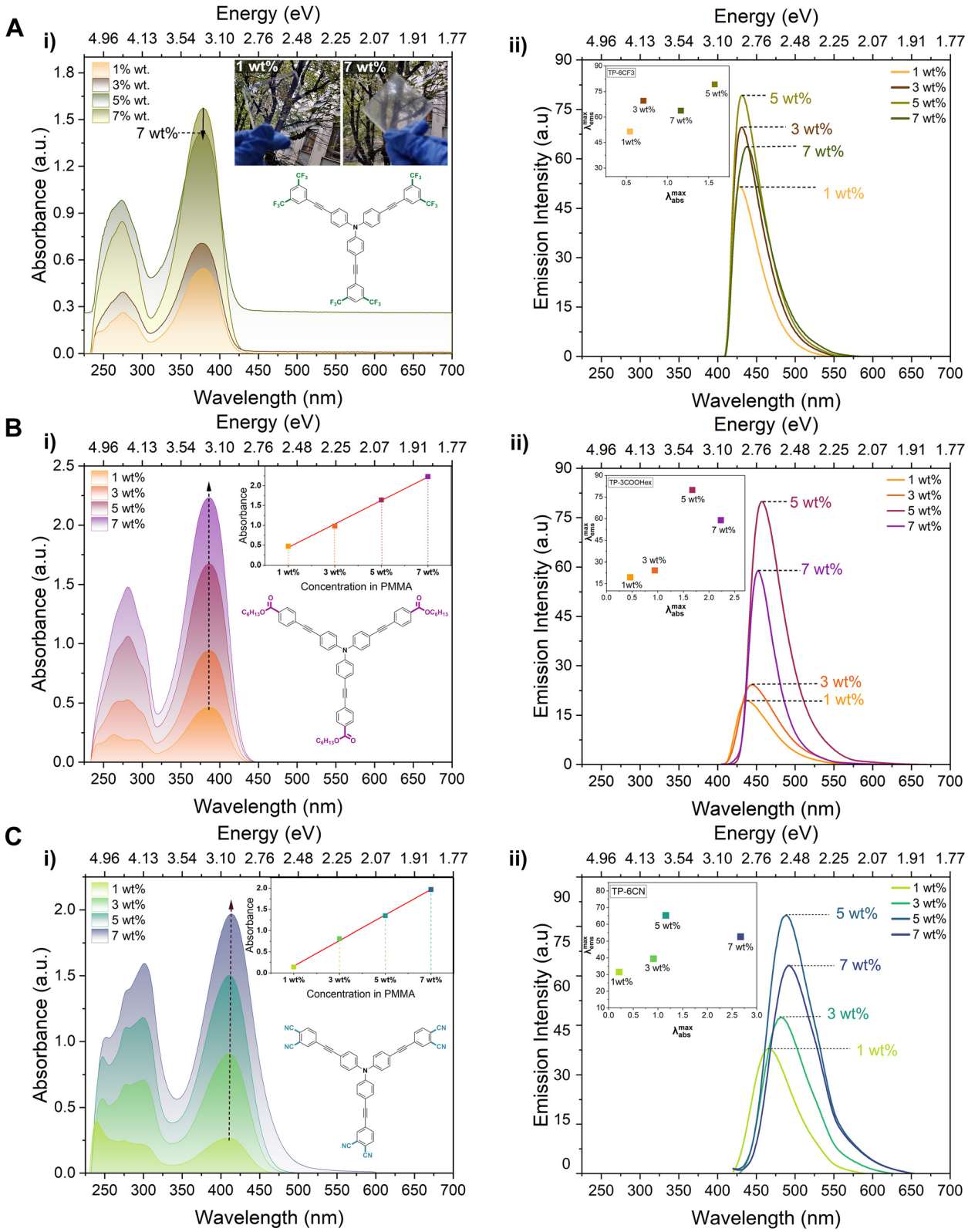

Fig. 2 (i) Absorption measurements for (A) TP-6CF3/PMMA, inset: photographs of TP-6CF3/PMMA 1 wt% and 7 wt%, (B) TP-3COOHex/PMMA and inset: maximum absorbance *vs.* concentration of TP-3COOHex on PMMA, and (C) TP-6CN/PMMA systems, inset: maximum absorbance *vs.* concentration of TP-6CN on PMMA, and (ii) emission measurements (front-face) with excitation wavelengths of (A) 375 nm for TP-6CF3/PMMA, (B) 385 nm for TP-3COOHex/PMMA, and (C) 410 nm for TP-6CN/PMMA, insets: correlation between absorption maxima (λ_{abs}^{max}) and emission maxima (λ_{ems}^{max}).

the branches of the two molecules, inducing a staggered configuration of the 2 + 2 and 3 + 3 dimers; in the case of TP-6CF3, the bulky $-CF_3$ terminations appeared to hinder the dispersion interaction between the branches and induced the antiparallel arrangement of two branches to minimize the total energy of the 1 + 1 dimer. There is no particular optoelectronic fingerprint of such different configurations, as indicated by the absorption spectra of dimers shown in Fig. S24 in the ESI,† in accordance with solid state measurements reported in Fig. 2. However, the peculiar arrangement of TP-6CF3 dimers suggests the possibility to form extended molecular networks driven by antiparallel interactions between branches that can account for the formation of large aggregates (such as those reported in the right panel of Fig. S24 in the ESI†).

3.2.2 Photophysical characterization of TPA-based/PMMA LSCs. The three TPA-based molecules were incorporated in a PMMA host matrix at increasing concentration levels and the absorption and emission characteristics were evaluated (Fig. 2). Specifically, TP-6CF3, TP-3COOHex and TP-6CN were maintained within the range of 1–7 wt%. The absorption spectra of the three systems exhibited two distinct electronic transitions: one at lower wavelengths (230–325 nm for TP-6CF3 and TP-3COOHex, and 230–350 nm for TP-6CN), and another one at higher wavelengths (325–450 nm for TP-3COOHex and TP-6CF3, and 350–500 nm for TP-6CN). Within the primary absorption peak observed in the 225–350 nm range, additional peaks are discernible, in line with the theoretical calculations discussed above. Interestingly, the absorption spectra for TP-3COOHex and TP-6CN exhibited a positive trend with increasing dye loading in PMMA, which could be fitted by the Beer–Lambert law (Fig. 2(B) and (C)). On the contrary, the films based on TP-6CF3 featured a significant loss of optical clarity and increased haziness for luminophore concentrations above 5 wt% (Fig. 2(A) (i) inset and Fig. S19 in the ESI†), yielding scattering and deviations from absorbance-concentration response linearity. This behavior is partially attributed to the limited compatibility of the CF_3-substituted TP-6CF3 with the PMMA matrix, due to its electron-withdrawing and lipophobic character, which promotes aggregation and light scattering at higher concentrations; possible mitigation strategies are discussed in the ESI† (Section S7) The front-face emission spectra showed the highest intensity at 5 wt% luminophore concentration for all systems, with a consistent pattern of emission increase from 1–5 wt% followed by a gradual decline at 7 wt% accompanied by a slight red-shift of the emission peak. This spectral shift is postulated to be the result of reabsorption and self-absorption phenomena.[48] Interestingly, the three systems were characterized by different emission ranges, resulting from the different substituents to the TPA core. In particular, a progressive bathochromic shift of the peak emission wavelength was observed going from TP-6CF3 to TP-3COOHex to TP-6CN, in agreement with the theoretical predictions (Fig. 1). The optical characteristics of all systems, including the maximum absorption wavelength (λ_{abs}^{max}) and maximum emission wavelength (λ_{ems}^{max}) and Stokes shift are reported in the ESI† (Table S7).

3.3 Photonic characterization of TPA-based/PMMA LSCs

3.3.1 External (η_{ext}) and internal (η_{int}) photon efficiencies. In order to validate the potential of TPA/PMMA-based LSC systems, both the external photon efficiency (η_{ext}) and the internal photon efficiency (η_{int}) were assessed under standard illumination conditions (AM 1.5G). η_{ext} and η_{int} were calculated from the experimental data according to eqn (S3) and (S4) (ESI†).[49] All the data of η_{ext} and η_{int} efficiencies along with the single-edge power output are reported in Table S8 (ESI†). Fig. 3 reveals a notably high η_{int} ($\approx$50–70%) in all systems at low luminophore concentrations (1 wt%), followed by a slight decrease for increasing luminophore loadings. In particular, a relatively constant value of $\eta_{int} \approx$ 45–50% is reached in TP-3COOHex and TP-6CN in the 3–5 wt% dye concentration range, which ranks among the best values reported in the literature for organic luminescent dyes.[13,50–54] A further enhancement in luminophore concentration led to a decrease in η_{int}, which was found to be prevailing for TP-6CN likely due to less favorable absorption–emission overlap and more pronounced reabsorption losses (as discussed

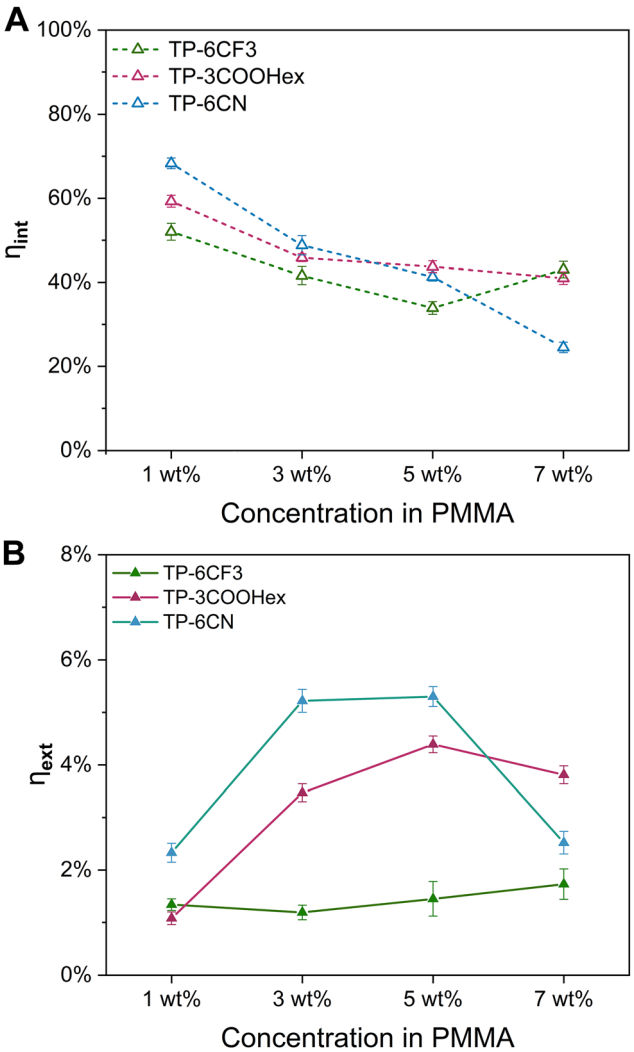

Fig. 3 (A) Internal and (B) external photon efficiency (η_{int} and η_{ext}, respectively) *versus* luminophore concentration.

in the following). On the other hand, lower efficiencies were observed for TP-6CF3 over the whole 1–5 wt% luminophore concentration range. It is worth noting that a slight increase in η_{int} is observed in the TP-6CF3/PMMA LSC system at a 7 wt% luminophore loading, likely stemming from the hazy appearance of this LSC system discussed previously, which is responsible for significant light scattering and overestimated photonic output. Both TP-COOHex and TP-6CN systems exhibited similar trends in terms of η_{ext}, with maximum response observed in the 3–5 wt% luminophore concentration range. In particular, the highest η_{ext} were found at 5 wt% dye loading, reaching values as high as η_{ext} = 5.3% and η_{ext} = 4.4% in TP-6CN/PMMA and TP-COOHex/PMMA, respectively, which are on a par with the highest values recently reported in the literature for devices of equivalent dimension and spectral response, and tested under similar light exposure conditions.[35,50,55,56] These results align well with the photophysical characteristics of these systems, as discussed previously. A further increase in dye concentration led to a progressive performance decrease, which may be associated with the emergence of detrimental self-absorption phenomena and scattering losses, as discussed in detail in the next section. As opposed to TP-COOHex and TP-6CN systems, TP-6CF3-based LSCs consistently exhibited lower η_{ext} values fluctuating between 1.2–1.75%, indicative of their inferior performance compared to the other systems.

3.3.2 Absorption efficiency (η_{abs}) and the radiative overlap (RO). To better understand the influence and extent of reabsorption losses on the performances of the TPA-based LSC devices, the absorption efficiency (η_{abs}) and the radiative overlap (RO) of LSC systems as a function of the luminophore concentration level were also estimated (eqn (S2) and (S5) in the ESI†). More specifically, η_{abs} measures the fraction of incident light absorbed by the LSC (*i.e.*, the match between the absorption response of the luminophore and the emission spectrum of the incident light), providing a direct estimate of the non-ideal optical properties of the luminophore. In contrast, RO quantifies the fraction of emitted light that can be re-absorbed by the luminophore due to the overlap between the absorbance and emission spectra. This parameter helps correlate the likelihood of reabsorption processes with the amount of luminescent species present in the system.

The data presented in Fig. 4(A) show a gradual increase in η_{abs} for the TP-3COOHex/PMMA and TP-6CN/PMMA systems at increasing luminophore loading, following an exponential

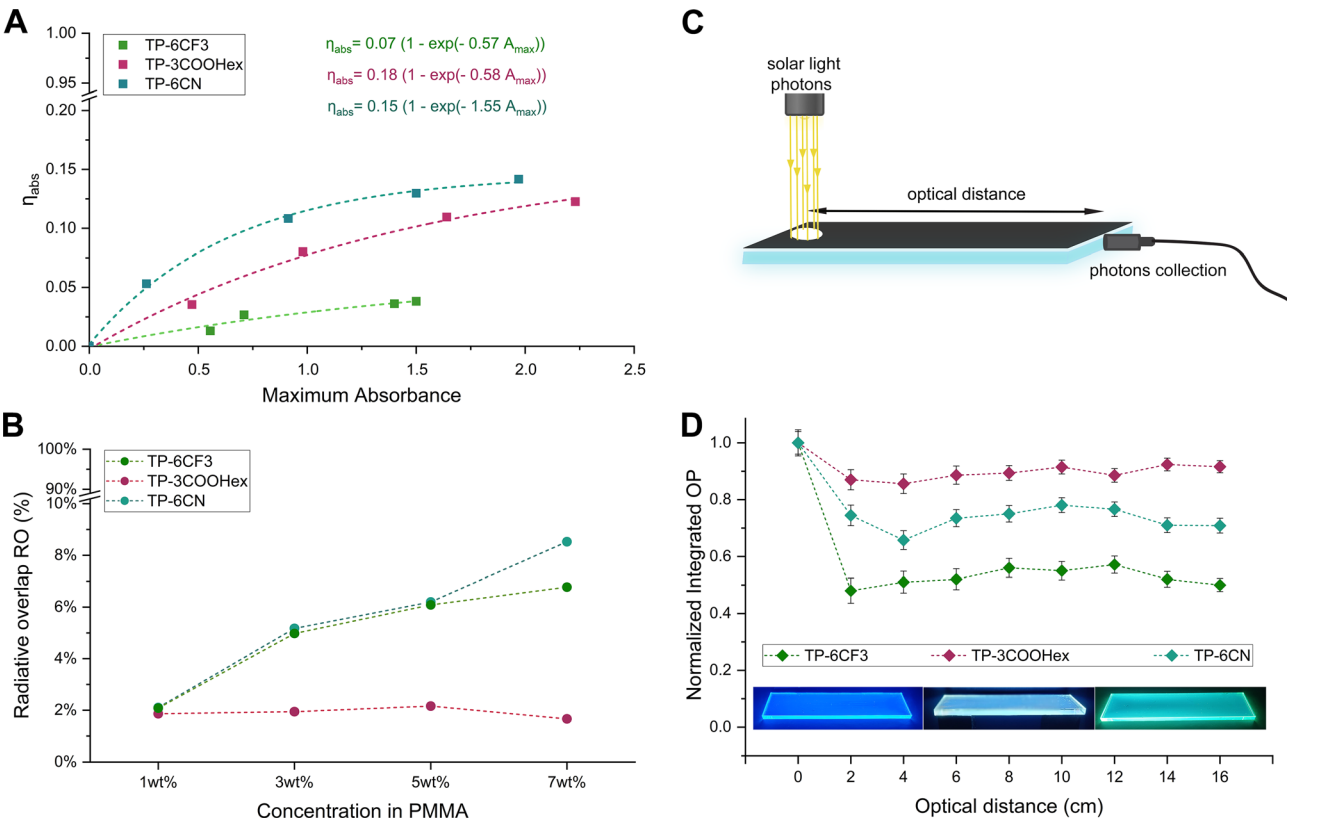

Fig. 4 (A) η_{abs} of the LSC system as a function of the maximum absorbance, $\lambda_{abs,max}$ = 377 nm (of the different concentrations) for TP-6CF3/PMMA, 386 nm for TP-3COOHex/PMMA and 410 nm for TP-6CN/PMMA. The dashed lines represent the exponential fits to the experimental results with the corresponding equations displayed on the figure (assuming no haze and scattering effects at 7 wt%), (B) radiative overlap (RO) *vs.* luminophore concentration of TPA-based/PMMA systems (assuming no haze and scattering effects at 7 wt%), (C) schematic of the experimental setup used to measure the decay in intensity of the integrated optical power output as a function of optical distance and (D) normalized intensity decay of the integrated optical power output, plotted as a function of optical distance from the illumination spot under 1 sun top illumination, with an inset showing images of 5 cm × 20 cm N-BK7 glass with the TP-6CF3/PMMA, TP-3COOHex/PMMA and TP-6CN/PMMA devices.

trend. In particular, the maximum theoretically achievable η_{abs} (for $A_{max} \rightarrow \infty$) was determined to be 0.13 and 0.16 for the TP-3COOHex/PMMA and TP-6CN/PMMA systems, respectively. In practical terms, this translates into a maximum absorption fraction equal to 13% and 16% of the total incident photons for TP-3COOHex/PMMA and TP-6CN/PMMA LSCs, respectively. Additionally, at any given maximum absorbance, η_{abs} was found to be larger for TP-6CN than for TP-3COOHex as a result of the larger overlap between the luminophore absorption spectra and the emission spectrum of the incident light source. In contrast, the TP-6CF3/PMMA system exhibited a much lower η_{abs} in the whole range of dye concentrations, in line with its optical/photophysics response. As shown in Fig. 4(B), all systems exhibited RO values lower than 2.5% at very low luminophore doping levels (<3 wt%), indicating that only a negligible fraction of the primary emitted photons is expected to be reabsorbed along the path to the edge at these concentrations. On the contrary, a gradual increase in RO was detected with increasing luminophore concentration in the case of TP-6CF3 and TP-6CN, reaching values of $\sim$8.5% and 6.5%, respectively, in highly concentrated LSC systems (7 wt% dye loading), as also observed in recent literature works.[57–59] Interestingly, systems based on TP-3COOHex were found to consistently maintain very low RO values (<2%) even at higher concentrations, thus explaining the excellent photonic response of TP-3COOHex/PMMA LSCs in terms of η_{int} across a wide range of dye concentrations (Fig. 3(A)). Indeed, a reduction in the overlap between absorption and emission spectra is key to achieving superior light-guiding response and increased edge-collection of the emitted luminescent light, thereby leading to LSCs of increased photonic efficiency.[60–62]

To further evaluate the contribution of reabsorption losses to the photonic response of the TPA-based LSCs, the net single-edge optical power output as a function of the optical path length d between the illumination spot (under 1 sun AM1.5G light) and the collecting edge was recorded for the three different systems, after correcting for scattering effects (Fig. S21 in the ESI†). For this test, high-optical-quality N-BK7 glass (with absorption coefficient $\alpha = 10^{-3}$ cm^{-1}) was used as waveguide, thus allowing the minimization of light transport losses given by waveguide absorption (Fig. 4(C)). As shown in Fig. 4(D), the net optical power output was found to remain in all cases relatively constant for photon travel distances d higher than 3–4 cm, thus indicating free propagation of emitted photons within the lightguide for larger devices and edge-collection with limited optical losses (the initial performance decay at short d can be attributed to geometric effects). In particular, a constant optical power output reduction of $\sim$25% and $\sim$45% was observed at $d > 5$ cm for TP-6CN and TP-6CF3 based systems, respectively (Fig. 4(C)). On the other hand, only a $\sim$10% decay was found in the case of TP-3COOHex, which can be correlated with the negligible RO observed in this system (Fig. 4(B)), ultimately resulting in limited photon self-absorption phenomena. Such limited reabsorption losses in TP-3COOHex based LSCs suggest their potential use for the fabrication of high-performance large-area devices.

4. Comprehensive analysis of visible transparency, power conversion efficiency, and photostability

Another important aspect to consider in the design of LSC systems is their visible appearance, which plays a crucial role in the architectural and aesthetic integration of these technologies in buildings. While the power conversion efficiency of these systems is paramount for energy generation, their aesthetic characteristics are equally critical for applications in windows and facades. For such systems to be seamlessly incorporated into building designs, transparency, color rendering, and visual comfort must meet specific architectural standards. To that end, parameters such as the average visible transmittance (AVT), the color rendering index (CRI), and the CIELAB color coordinates (a^*, b^*) are essential in determining their suitability for integration into modern building structures.[63–66] The AVT determines the level of transparency, which is crucial for window applications, while the CRI and the CIELAB color coordinates help assess how well the system renders colors and how tinted the device will appear to human eyes. For reference, a typical clear double-pane insulated glass unit has an AVT of nearly 80%.[67] The AVT spectrum for residential windows spans from 15% for highly tinted glass to 90% for commonly clear glass. In essence, glass with AVT values surpassing 60% exudes clarity, while values below 50% are indicative of dark, colored, or reflective attributes.[67,68]

The CRI graph for the three TPA-based devices at varying luminophore concentrations is presented in Fig. 5(A) (the resulting x, y coordinates in the CIE 1931 graph and in the a^*b^* color space are reported in Table S13 in the ESI†). All systems tend towards the blue range of the visible spectrum, except TP-6CN, which transitions towards the yellow at higher concentrations. This transition is corroborated by the visual appearance of the coated glass, which exhibits a more yellowish hue compared to the other systems, as illustrated in Fig. 5(B).

The AVT values were calculated for each system based on an optimized luminophore concentration of 5 wt%, as inferred from photonic characterization (eqn (S6) in the ESI†). As shown in Fig. 5(C) and summarized in Table 2, all TPA/PMMA-based systems consistently maintained AVT values of $\sim$90% or higher, demonstrating a very high level of transparency. Such transparency makes these LSC devices ideal for architectural integration, as they blend seamlessly into building designs without significantly altering their visual appearance, while simultaneously serving a functional role (light collection, emission and conversion).

To investigate the potential of these systems in the area of building-integrated PVs, the corresponding LSC-PV devices were assembled and tested under 1 sun AM1.5G simulated sunlight. To that end, in addition to the LSC device power conversion efficiency, η_{dev}, the light utilization efficiency (LUE = AVT·η_{dev}) was also computed as a more comprehensive measure of the trade-off between the aesthetic (visible transparency) and the functional (power conversion efficiency) response of the device (see ESI† for details on calculations).[69]

As shown in Table 2, the TP-6CF3/PMMA LSC device exhibited the poorest PV response, achieving a short-circuit current (I_{SC}) of 4.63 mA and a maximum output power (P_{max}) of 10.22 mW, resulting in an overall efficiency (η_{dev}) of 0.27%. This behavior is in line with the optical characteristics (Fig. 2) and

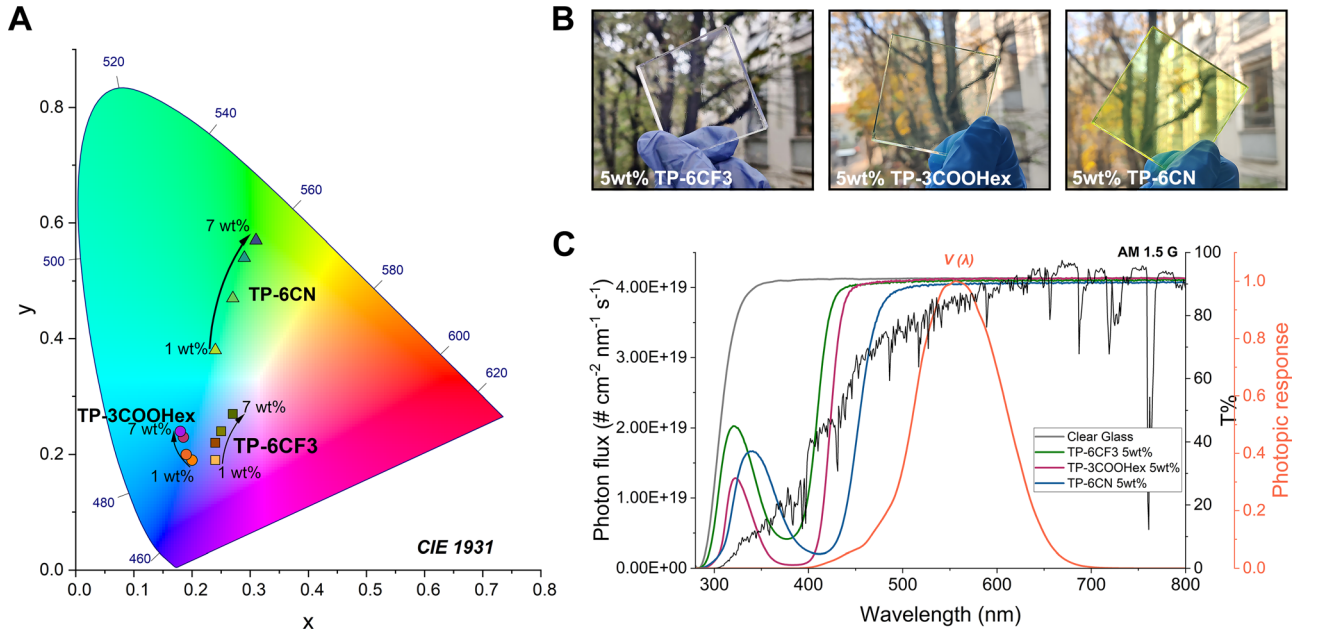

Fig. 5 (A) Color coordinates (CIE 1931 Uniform Color Space) of TP-6CF3/PMMA (square symbols), TP-COOHex/PMMA (circles), and TP-6CN/PMMA (triangles) LSC systems at increasing luminophore concentration, (B) photographs of the LSC devices with TP-6CF3/PMMA, TP-COOHex/PMMA, and TP-6CN/PMMA LSCs with 5 wt% content of fluorophore for all systems and (C) transmittance spectra of various TPA-based/PMMA LSC devices at 5 wt% fluorophore content, AM 1.5G photon flux and photopic response function $V(\lambda)$.

Table 2 PV parameters and efficiencies of the fabricated TPA-based/PMMA LSC devices

Device	I_{SC} (mA)	P_{max} (mW)	η_{dev} (%)	AVT (%)	LUE (%)
TP-6CF3	4.63 ± 0.02	10.23 ± 0.04	0.27 ± 0.006	91.58	0.25
TP-3COOHex	5.77 ± 0.01	12.98 ± 0.07	0.34 ± 0.003	91.54	0.31
TP-6CN	5.89 ± 0.02	13.37 ± 0.09	0.36 ± 0.003	89.54	0.32

photonic response (Fig. 3) of TP-6CF3, which were also found to yield the lowest η_{abs} (poor spectral match with sunlight emission) and the highest RO (non-negligible reabsorption losses) (Fig. 4). On the other hand, both TP-3COOHex/PMMA and TP-6CN/PMMA LSC devices demonstrated better performance with comparable PV response, in agreement with their optical characteristics. More specifically, I_{SC} values in the 5.77–5.89 mA range and maximum power density P_{max} of 12.98–13.37 mW were recorded for these systems, leading to η_{dev} = 0.34% and 0.36% for TP-3COOHex/PMMA and TP-6CN/PMMA LSC devices, respectively.[2,70]

These values are comparable to those recently obtained on LSC devices based on Si-PV cells and incorporating organic luminophores exhibiting similar absorption/emission spectral characteristics.[35,71] In view of their potential application in outdoor contexts, the photostability of all TPA/PMMA-based LSC systems was preliminarily evaluated by monitoring their spectral output under continuous UV-A irradiation (radiative input power = 54.6 mW cm^{-2}) in air at a temperature of 50 °C.

The single-edge output power of TPA-PMMA LSCs with luminophore concentrations of 5 wt% for each TPA luminophore, was collected every 5 minutes (see Fig. S22, ESI†). Importantly, despite the aggressive exposure conditions, all devices demonstrated good retention of their initial optical response, confirming their overall photostability. These results, combined with the excellent photonic and PV response of these systems (especially TP-3COOHex and TP-6CN) and their favorable aesthetic characteristics, make these luminophores particularly attractive for real-world LSC application scenarios.

5. Conclusions

In this study, a series of tris-(4-phenylethynyl-phenyl)-amine-based luminescent molecules was presented for use as high-efficiency luminophores in LSCs. These luminescent species were synthesized in three-steps at ambient temperature using non-toxic propane-1,2-diol as the primary reaction medium, providing a sustainable synthetic pathway characterized by an E-factor as low as <190. The characteristic symmetrical D–(π–A)$_3$ donor–acceptor architecture of these TPA derivatives (TP-6CF3, TP-3COOHex, and TP-6CN, bearing 3,5-bis(trifluoromethyl)phenyl, hexyl-4-benzoate, and 3,4 dicyanophenyl moieties, respectively) enabled the fine tuning of their optical response for maximized Stokes shift, favorable match with the solar spectrum and efficient emission, yielding maximum PLQY values in the 70–80% range. In addition, DFT calculations highlighted clear correlations between molecular arrangement and optical properties, which were reflected in the experimental characteristics of the obtained molecules.

The incorporation of such luminescent derivatives in PMMA matrices at increasing concentration enabled the systematic investigation of their photonic and PV response in LSC devices under simulated sunlight. In particular, systems based on TP-3COOHex and TP-6CN were found to attain η_{int} as high as 45–50% and η_{ext} in the 4.4–5.3% range, which aligned well with

their photophysical characteristics. On the contrary, TP-6CF3-based LSCs consistently exhibited inferior photonic response over the whole luminophore concentration range investigated, as a result of the less favorable optical characteristics of this luminescent species. Similarly, higher PV efficiencies η_{dev} were found in TP-3COOHex and TP-6CN systems *vs.* TP-6CF3. These trends were also confirmed by the results of a comprehensive analysis of transmission, reabsorption and light-transport losses carried out on these LSC devices.

In conclusion, the particularly straightforward and affordable synthetic pathway to access these TPA-based luminophores, combined with the excellent photonic and PV response of the corresponding LSC devices (especially TP-3COOHex and TP-6CN) and with their favorable aesthetic characteristics (the selective absorption in the near-UV and blue region, combined with high average visible transmittance (AVT $\sim$ 90%)), make these systems particularly attractive candidates for future building-integrated LSC applications.

Author contributions

E. T.: investigation, data curation, writing – original draft, V. R.: investigation (synthesis and characterization), data curation, writing – original draft, G. R. R.: investigation (device fabrication and characterization), data curation, writing – original draft, S. T.: data curation, supervision, writing – review & editing, G. M. and F. P.: theoretical calculations, data curation, writing – review & editing, D. C.: investigation (characterization), data curation, writing – review & editing, C. B.: investigation (characterization), data curation, writing – review & editing, G. Z. and G. G.: conceptualization, funding acquisition, supervision, writing – review & editing. The manuscript was written through contributions of all the authors. All the authors have given approval to the final version of the manuscript.

Data availability

The data supporting this article have been included as part of the ESI.†

Conflicts of interest

The author declares that there are no conflicts of interest related to this publication.

Acknowledgements

This project has received funding from the Italian Ministry of University and Research (MUR) (PRIN 2022 Prot. 2022BREBFN, project: NIR+). Gianmarco Griffini and Elisavet Tatsi gratefully acknowledge financial contribution from Fondazione Cariplo (Ref. 2023-1656, project: PHASMA). Giuseppe Mattioli and Francesco Porcelli also gratefully acknowledge financial contribution from ICSC-Centro Nazionale di Ricerca in High Performance Computing, Big Data and Quantum Computing, funded by European Union-NextGenerationEU (grant CN00000013). Venanzio Raglione gratefully acknowledges funding from HORIZON EUROPE under the project "Fast plasma-assisted perovskite crystallization for high efficiency lead-free perovskite thin film photovoltaics" (SMART-LINE PV), grant agreement no. 101122327.

Notes and references

1 S. Castelletto and A. Boretti, *Nano Energy*, 2023, **109**, 108269.
2 E. Tatsi, M. De Marzi, L. Mauri, A. Colombo, C. Botta, S. Turri, C. Dragonetti and G. Griffini, *Macromol. Rapid Commun.*, 2024, **45**, 2300724.
3 C. Yang, M. Moemeni, M. Bates, W. Sheng, B. Borhan and R. R. Lunt, *Adv. Opt. Mater.*, 2020, **8**, 1901536.
4 C. Lee, H. Cho, J. Ko, S. Kim, Y. Ko, S. Park, Y. Kang, Y. J. Yun and Y. Jun, *Opt. Express*, 2022, **30**, 37085.
5 G. Griffini, L. Brambilla, M. Levi, M. Del Zoppo and S. Turri, *Sol. Energy Mater. Sol. Cells*, 2013, **111**, 41–48.
6 S. Han, J. Wen, Z. Cheng, G. Chen, S. Jin, C. Shou, H.-C. Kuo and C.-C. Tu, *Opt. Express*, 2022, **30**, 26896.
7 J. Choi, K. Kim and S.-J. Kim, *Sci. Rep.*, 2021, **11**, 13833.
8 M. D. J. Fimbres-Romero, Á. Flores-Pacheco, M. E. Álvarez-Ramos and R. Lopez-Delgado, *ACS Omega*, 2024, **9**, 28008–28017.
9 G. Fortunato, E. Tatsi, F. Corsini, S. Turri and G. Griffini, *ACS Appl. Polym. Mater.*, 2020, **2**, 3828–3839.
10 E. Tatsi, G. Fortunato, B. Rigatelli, G. Lyu, S. Turri, R. C. Evans and G. Griffini, *ACS Appl. Energy Mater.*, 2020, **3**, 1152–1160.
11 P. Meti, F. Mateen, D. Y. Hwang, Y. E. Lee, S. K. Hong and Y. D. Gong, *Dyes Pigm.*, 2022, **202**, 110221.
12 S. Mattiello, A. Sanzone, F. Bruni, M. Gandini, V. Pinchetti, A. Monguzzi, I. Facchinetti, R. Ruffo, F. Meinardi, G. Mattioli, M. Sassi, S. Brovelli and L. Beverina, *Joule*, 2020, **4**, 1988–2003.
13 C. Ceriani, F. Corsini, G. Mattioli, S. Mattiello, D. Testa, R. Po, C. Botta, G. Griffini and L. Beverina, *J. Mater. Chem. C*, 2021, **9**, 14815–14826.
14 R. Pervin, E. M. Gholizadeh, K. P. Ghiggino and W. W. H. Wong, *J. Mater. Chem. C*, 2024, **12**, 8498–8507.
15 E. Rosadoni, F. Bellina, M. Lessi, C. Micheletti, F. Ventura and A. Pucci, *Dyes Pigm.*, 2022, **201**, 110262.
16 A. Picchi, K. Kantarod, M. Ilarioni, M. Carlotti, P. Leowanawat and A. Pucci, *Mater. Today Energy*, 2024, **44**, 101646.
17 E. Tatsi, A. Nitti, D. Pasini and G. Griffini, *Nanoscale*, 2024, **16**, 15502–15514.
18 A. Pucci, *Isr. J. Chem.*, 2018, **58**, 837–844.
19 F. Corsini, A. Nitti, E. Tatsi, G. Mattioli, C. Botta, D. Pasini and G. Griffini, *Adv. Opt. Mater.*, 2021, **9**, 2100182.
20 D. O. Balakirev, A. N. Solodukhin, S. M. Peregudova, E. A. Svidchenko, N. M. Surin, Y. V. Fedorov, S. A. Ponomarenko and Y. N. Luponosov, *Dyes Pigm.*, 2023, **208**, 110777.
21 M. Fang, H. Lu, R. Li, W. Wei, L. Mao, T. Christoforo, G. Chen, Y. Guan, X. Pei, Q. Chen, M. Tian and Y. Wei, *Chem. Eng. J. Adv.*, 2022, **12**, 100411.
22 F. Mateen, T. G. Hwang, L. F. Boesel, W. J. Choi, J. P. Kim, X. Gong, J. M. Park and S. K. Hong, *Int. J. Energy Res.*, 2021, **45**, 17971–17981.

23 B. Zhao, H. Ma, H. Jia, M. Zheng, K. Xu, R. Yu, S. Qu and Z. Tan, *Angew. Chem., Int. Ed.*, 2023, **62**, e202301651.
24 A. Brzeczek, K. Karon, H. Higginbotham, R. G. Jędrysiak, M. Lapkowski, K. Walczak and S. Golba, *Dyes Pigm.*, 2016, **133**, 25–32.
25 A. Karak, S. K. Manna and A. K. Mahapatra, *Anal. Methods*, 2022, **14**, 972–1005.
26 T. Sun, Z. Gong, J. Shao and Y. Zhong, *Chin. J. Chem.*, 2020, **38**, 1515–1520.
27 K. R. Justin Thomas, J. T. Lin, Y.-T. Tao and C.-W. Ko, *Chem. Mater.*, 2002, **14**, 1354–1361.
28 A. Meli, B. Ebenhoch, K. Kutonova, A. Bihlmeier, A. Feyrer, E. Deck, F. Breher, M. Nieger, A. Colsmann and S. Bräse, *Synth. Met.*, 2019, **256**, 116138.
29 X. Wang, D. Wang, G. Zhou, W. Yu, Y. Zhou, Q. Fang and M. Jiang, *J. Mater. Chem.*, 2001, **11**, 1600–1605.
30 P. Blanchard, C. Malacrida, C. Cabanetos, J. Roncali and S. Ludwigs, *Polym. Int.*, 2019, **68**, 589–606.
31 R. Fuentes Pineda, Y. Zems, J. Troughton, M. R. Niazi, D. F. Perepichka, T. Watson and N. Robertson, *Sustainable Energy Fuels*, 2020, **4**, 779–787.
32 J. Wang, K. Liu, L. Ma and X. Zhan, *Chem. Rev.*, 2016, **116**, 14675–14725.
33 C. Le Droumaguet, A. Sourdon, E. Genin, O. Mongin and M. Blanchard-Desce, *Chem. – Asian J.*, 2013, **8**, 2984–3001.
34 C. Papucci, A. Dessì, C. Coppola, A. Sinicropi, G. Santi, M. Di Donato, M. Taddei, P. Foggi, L. Zani, G. Reginato, A. Pucci, M. Calamante and A. Mordini, *Dyes Pigm.*, 2021, **188**, 109207.
35 M. Bartolini, C. Micheletti, A. Picchi, C. Coppola, A. Sinicropi, M. Di Donato, P. Foggi, A. Mordini, G. Reginato, A. Pucci, L. Zani and M. Calamante, *ACS Appl. Energy Mater.*, 2023, **6**, 4862–4880.
36 X. Li, J. Qi, J. Zhu, Y. Jia, Y. Liu, Y. Li, H. Liu, G. Li and K. Wu, *J. Phys. Chem. Lett.*, 2022, **13**, 9177–9185.
37 Y. Li, J. Olsen, K. Nunez-Ortega and W.-J. Dong, *Sol. Energy*, 2016, **136**, 668–674.
38 K. Li, W. Qin, D. Ding, N. Tomczak, J. Geng, R. Liu, J. Liu, X. Zhang, H. Liu, B. Liu and B. Z. Tang, *Sci. Rep.*, 2013, **3**, 1150.
39 B. Zhang, J. L. Banal, D. J. Jones, B. Z. Tang, K. P. Ghiggino and W. W. H. Wong, *Mater. Chem. Front.*, 2018, **2**, 615–619.
40 V. Raglione, F. Palmeri, G. Mattioli, F. Porcelli, D. Caschera and G. Zanotti, *Chem. – Eur. J.*, 2024, **30**, e202402901.
41 S. Mondal, A. A. Arifa and P. Biswas, *Catal. Lett.*, 2017, **147**, 2783–2798.
42 J. B. Restrepo, C. D. Paternina-Arboleda and A. J. Bula, *Energies*, 2021, **14**, 5081.
43 Y. Tao, C. Bu, L. Zou, Y. Hu, Z.-J. Zheng and J. Ouyang, *Biotechnol. Biofuels*, 2021, **14**, 216.
44 K. Kang, L. Li, M. Zhang, X. Miao, L. Lei and C. Xiao, *Inorg. Chem.*, 2022, **61**, 11463–11470.
45 R. A. Sheldon, *Chem. Ind.*, 1992, 903–906.
46 R. A. Sheldon, *ACS Sustainable Chem. Eng.*, 2018, **6**, 32–48.
47 E. Ghiglietti, E. A. Incarbone, S. Mattiello and L. Beverina, *Eur. J. Org. Chem.*, 2024, e202400223.
48 S. Li and S. Haussener, *J. Quant. Spectrosc. Radiat. Transfer*, 2024, **319**, 108957.
49 M. G. Debije, R. C. Evans and G. Griffini, *Energy Environ. Sci.*, 2021, **14**, 293–301.
50 D.-Y. Hwang, P. Meti, F. Mateen, D.-S. Lee, Y.-J. Yang, J.-S. Eom, J.-W. Shin, S. M. H. Qaid, Y.-D. Gong and S.-K. Hong, *Dyes Pigm.*, 2024, **221**, 111775.
51 Y. Zhang, Z. Zheng, Z. Gan, R. Huang and X. Zhang, *Small Sci.*, 2024, **4**, 2400121.
52 S. Mattiello, A. Sanzone, F. Bruni, M. Gandini, V. Pinchetti, A. Monguzzi, I. Facchinetti, R. Ruffo, F. Meinardi, G. Mattioli, M. Sassi, S. Brovelli and L. Beverina, *Joule*, 2020, **4**, 1988–2003.
53 M. Moser, A. Wadsworth, N. Gasparini and I. McCulloch, *Adv. Energy Mater.*, 2021, **11**, 2100056.
54 F. Corsini, A. Nitti, E. Tatsi, G. Mattioli, C. Botta, D. Pasini and G. Griffini, *Adv. Opt. Mater.*, 2021, **9**, 2100182.
55 P. Meti, F. Mateen, D. Y. Hwang, Y.-E. Lee, S.-K. Hong and Y.-D. Gong, *Dyes Pigm.*, 2022, **202**, 110221.
56 A. Kathiravan, F. Mateen, P. Gopinath, D.-Y. Hwang, S.-K. Hong and S. M. H. Qaid, *Dyes Pigm.*, 2024, **222**, 111869.
57 C. Yang, M. Moemeni, M. Bates, W. Sheng, B. Borhan and R. R. Lunt, *Adv. Opt. Mater.*, 2020, **8**, 1901536.
58 N. S. Makarov, D. Korus, D. Freppon, K. Ramasamy, D. W. Houck, A. Velarde, A. Parameswar, M. R. Bergren and H. McDaniel, *ACS Appl. Mater. Interfaces*, 2022, **14**, 29679–29689.
59 N. C. Giebink, G. P. Wiederrecht and M. R. Wasielewski, *Nat. Photonics*, 2011, **5**, 694–701.
60 M. G. Debije, R. C. Evans and G. Griffini, *Energy Environ. Sci.*, 2021, **14**, 293–301.
61 Y. Zhou, D. Benetti, Z. Fan, H. Zhao, D. Ma, A. O. Govorov, A. Vomiero and F. Rosei, *Adv. Energy Mater.*, 2016, **6**, aenm. 201670067.
62 M. A. Hernández-Rodríguez, S. F. H. Correia, R. A. S. Ferreira and L. D. Carlos, *J. Appl. Phys.*, 2022, **131**, 140901.
63 I. Motta, G. Bottaro, M. Rando, M. Rancan, R. Seraglia and L. Armelao, *J. Mater. Chem. A*, 2024, **12**, 22516–22527.
64 W. G. J. H. M. Van Sark, T. A. De Bruin, R. Terricabres Polo and C. De Mello Donegá, in *New Concepts in Solar and Thermal Radiation Conversion V*, ed. J. N. Munday and P. Bermel, SPIE, San Diego, United States, 2023, p. 1.
65 Z. Song, Z. Zheng, Y. Zhang, X. Cao, S. Li, H. Zhang, C. Luo, Y. Li and X. Zhang, *J. Lumin.*, 2023, **256**, 119622.
66 C. Yang, M. C. Barr and R. R. Lunt, *Phys. Rev. Appl.*, 2022, **17**, 034054.
67 C. Yang, D. Liu, M. Bates, M. C. Barr and R. R. Lunt, *Joule*, 2019, **3**, 1803–1809.
68 C. J. Traverse, R. Pandey, M. C. Barr and R. R. Lunt, *Nat. Energy*, 2017, **2**, 849–860.
69 Q. Zheng, H. Zhou, S. Du, P. Chen, J. Huang, H. Deng, J. Wu, C. Zhang, W. Wang and S. Cheng, *J. Mater. Sci.: Mater. Electron.*, 2024, **35**, 384.
70 J. Huang, J. Zhou, E. Jungstedt, A. Samanta, J. Linnros, L. A. Berglund and I. Sychugov, *ACS Photonics*, 2022, **9**, 2499–2509.
71 F. Mateen, N. Lee, S. Y. Lee, S. Taj Ud Din, W. Yang, A. Shahzad, A. K. Kaliamurthy, J.-J. Lee and S.-K. Hong, *Polymers*, 2021, **13**, 3770.